Available online at www.sciencedirect.com
ScienceDirect
Journal of Solid State Chemistry 179 (2006) 2954–2963
JOURNAL OF SOLID STATE CHEMISTRY
www.elsevier.com/locate/jssc

X-ray powder diffraction studies and thermal behaviour of $NaK_2B_9O_{15}$, $Na(Na_{.17}K_{.83})_2B_9O_{15}$, and $(Na_{.80}K_{.20})K_2B_9O_{15}$

R. Bubnova[a], B. Albert[b], M. Georgievskaya[a], M. Krzhizhanovskaya[c], K. Hofmann[b], S. Filatov[c,*]

[a]*Grebenshchikov Institute of Silicate Chemistry, RAS, St. Petersburg, 199155, Russia*
[b]*Eduard-Zintl-Institut fur Anorganische und Physikalische Chemie, Technische Universität Darmstadt, 64287 Darmstadt, Germany*
[c]*Department of Crystallography, St. Petersburg State University, St. Petersburg 199034, Russia*

Received 28 March 2006; received in revised form 26 May 2006; accepted 11 June 2006
Available online 27 June 2006

Abstract

The crystal structures of $NaK_2B_9O_{15}$ ($a = 9.1158(1)$ Å, $b = 6.6246(1)$ Å, $c = 20.6812(3)$ Å, $\beta = 94.080(1)^\circ$, $R_p = 0.047$, $R_{wp} = 0.059$, $R_B = 0.026$), $Na(Na_{.17}K_{.83})_2B_9O_{15}$ ($a = 9.0559(1)$ Å, $b = 6.6170(1)$ Å, $c = 20.5833(3)$ Å, $\beta = 94.228(2)^\circ$, $R_p = 0.053$, $R_{wp} = 0.068$, $R_B = 0.026$), and $(Na_{.80}K_{.20})K_2B_9O_{15}$ ($a = 9.1534(1)$ Å, $b = 6.6296(1)$ Å, $c = 20.7422(3)$ Å, $\beta = 94.071(1)^\circ$, $Z = 4$, $R_p = 0.041$, $R_{wp} = 0.052$, $R_B = 0.023$) were refined in the monoclinic space groups $P2_1/c$ ($Z = 4$) using X-ray powder diffraction data and the Rietveld method. These nonaborates are isostructural to $K_3B_9O_{15}$. Their crystal structure consists of a three-dimensional open framework built up from three crystallographically independent triborate groups. The alkali metal cations are located on three different sites in the voids of the framework. High-temperature X-ray diffraction studies show that $NaK_2B_9O_{15}$ decomposes at about 700 °C in accordance with the peritectic reaction $NaK_2B_9O_{15} \leftrightarrow K_5B_{19}O_{31}$ + liquid. The thermal expansion of $NaK_2B_9O_{15}$ and $Na(Na_{.17}K_{.83})_2B_9O_{15}$ is highly anisotropic. A similarity of the thermal and compositional (Na–K substitution) deformations of $NaK_2B_9O_{15}$ is revealed: heating of $NaK_2B_9O_{15}$ by 1 °C leads to the same deformations of the crystal structure as increasing the amount of K atoms in $(Na_{1-x}K_x)_3B_9O_{15}$ by 0.04 at% K.
© 2006 Elsevier Inc. All rights reserved.

Keywords: Borate; Solid solution; Rietveld structure refinement; Compositional deformation; Thermal deformation

1. Introduction

Sodium and potassium borates are traditionally used in manufacturing various glasses. Some of these borates have received great attention recently owing to their non-linear optical [1–4], piezoelectric [5], luminescent and other useful properties. Among the borates of univalent metals with $1R_2O{:}3B_2O_3$ stoichiometry (R = Li, Na, K, Rb, Cs, Tl) there are several compounds (e.g., LiB_3O_5 [6], CsB_3O_5 [7,8], $CsLiB_6O_{10}$ [9], TlB_3O_5 [10]) with excellent non-linear optical properties. Other triborates, such as the non-centrosymmetric α-RbB_3O_5 [11] and β-RbB_3O_5 [12], can be considered as potential non-linear optical materials. The frameworks of these triborate structures are topologically identical, and all of them are made up of the same triborate groups composed of two corner-sharing triangles connected to one tetrahedron.

Unlike the *ternary* triborates of univalent metals, whose crystal structures are well-known, the structure of only one *quarternary*, mixed cation triborate, $CsLiB_6O_{10}$, has been determined. In the context of searching for new anhydrous alkali metal triborates with promising structures and properties the pseudo-ternary (or pseudo-binary) system NaB_3O_5–KB_3O_5 has now been investigated, and the results of the structural studies will be reported below.

The compounds NaB_3O_5 and KB_3O_5 were first reported in phase diagrams of the Na_2O–B_2O_3 and K_2O–B_2O_3

*Corresponding author.
E-mail addresses: rimma_bubnova@mail.ru (R. Bubnova), albert@ac.chemie.tu-darmstadt.de (B. Albert), m.georgievskaya@mail.ru (M. Georgievskaya), filatov@crystal.pu.ru (S. Filatov).

0022-4596/$ - see front matter © 2006 Elsevier Inc. All rights reserved.
doi:10.1016/j.jssc.2006.06.020

systems [13,14]. The structures of the β- [15] and α-NaB_3O_5 [16] modifications crystallize in the monoclinic crystal system, space groups $P2_1/c$. Triclinic cell parameters of KB_3O_5 were reported in [17]. We later solved its structure in the monoclinic crystal system, space group $P2_1/c$ [18]. It is characterised by a boron–oxygen framework that is formed by triborate rings $[B_3O_5]^-$ as in most alkali triborates. Three independent cationic sites are located in channels of the framework. Since there are nine independent boron atoms, the compound should be described as a nonaborate, $K_3B_9O_{15}$, in accordance with the modern classification of borates [19]. The kinetics of its decomposition into two phases $K_5B_{19}O_{31}$ and $K_2B_4O_7$ at 660 °C were investigated in detail by annealing and quenching techniques [20].

Our preliminary studies [21,22] have shown that a solid solution exists in the $(Na_{1-x}K_x)_3B_9O_{15}$ system with a range of compositions for $x \approx 0.5$–1.0 (NaB_3O_5–KB_3O_5 pseudo-binary system). The decomposition of these solid solutions was examined by annealing techniques as well as by differential scanning calorimetry (DSC) [21]. Since the nonaborates investigated decompose forming other phases from the Na_2O–K_2O–B_2O_3 system, new phase relationships are expected and searched for using high-temperature X-ray diffraction (HTXRD) data as well as the DSC data. Here, we present the crystal structures of the new compounds, $NaK_2B_9O_{15}$, $Na(Na_{.17}K_{.83})_2B_9O_{15}$, and $(Na_{.8}K_{.2})K_2B_9O_{15}$ determined from X-ray powder diffraction data, and a comparison of these phases after heating or substitution of the cations. The Na–K distribution over the three independent sites is of special interest to our investigations. Phase relationships and melting behaviour are studied by means of HTXRD and DSC.

2. Experimental technique

2.1. Synthesis and heat treatment

The samples under investigation (Table 1, Fig. 5) were prepared by glass crystallization. First the ceramic pellets were prepared from stoichiometric mixtures of H_3BO_3 (high-purity grade) and dried Na_2CO_3 and K_2CO_3 (analytical grade). The pellets were pressed at a pressure of 70–100 kg/cm^2 and heat-treated at 670 °C for 20 h. To prepare glasses the pellets were placed in platinum crucibles and a hot Globar-heater furnace and held at a temperature of 1000 °C for 0.5–1 h. The melt was then poured onto a cold steel plate. This resulted in the formation of a transparent colourless glass. The chemical analysis of selected glasses showed that their composition is in good agreement with the batch composition. For example, the NaB_3O_5 glass contained 25.53 mol% Na_2O and 74.45 mol% B_2O_3, and the KB_3O_5 glass has 25.45 mol% K_2O and 74.65 mol% B_2O_3. To prepare crystalline powders the glasses were heat-treated in a furnace at temperatures between 500 and 800 °C for 0.5–50 h.

Table 1
Products of glass crystallization at 600 °C in the Na_2O–K_2O–B_2O_3 system

Sample	Composition (mol %) Na_2O–K_2O–B_2O_3	Crystalline phases (from powder X-ray diffraction)
1	00.0–25.4–74.6	$K_3B_9O_{15}$
2	02.5–22.5–75.0	$(Na_{.30}K_{.70})K_2B_9O_{15}$
3	06.5–18.4–75.1	$(Na_{.80}K_{.20})K_2B_9O_{15}$ + 3.6 mol% $K_5B_{19}O_{31}$
4	08.1–16.8–75.1	$NaK_2B_9O_{15}$ + 1.7 mol% $K_5B_{19}O_{31}$
5	08.2–16.8–75.0	$NaK_2B_9O_{15}$
6	11.4–13.6–75.0	$Na(Na_{.17}K_{.83})_2B_9O_{15}$ + 2.5 mol% β-NaB_3O_5
7	12.5–12.5–75.0	$Na(Na_{.17}K_{.83})_2B_9O_{15}$ + β-NaB_3O_5
8	13.8–11.2–75.0	$Na(Na_{.17}K_{.83})_2B_9O_{15}$ + β-NaB_3O_5
9	16.2–08.2–75.0	$Na(Na_{.17}K_{.83})_2B_9O_{15}$ + β-NaB_3O_5
10	18.8–06.2–75.0	β-NaB_3O_5 + $Na(Na_{.17}K_{.83})_2B_9O_{15}$
11	22.5–02.5–75.0	β-NaB_3O_5 + $Na(Na_{.17}K_{.83})_2B_9O_{15}$
12	25.5–00.0–74.5	β-NaB_3O_5
13	03.0–25.0–72.0	$(Na_{.80}K_{.20})K_2B_9O_{15}$ + $K_2B_4O_7$
14	10.0–18.0–72.0	$NaK_2B_9O_{15}$ + $K_2B_4O_7$
15	13.0–10.0–77.0	β-NaB_3O_5 + traces of $K_5B_{19}O_{31}$
16	00.0–20.8–79.2	$K_5B_{19}O_{31}$
17	00.0–33.3–66.7	$K_2B_4O_7$

2.2. Structure refinement

The diffraction data for $NaK_2B_9O_{15}$, $Na(Na_{.17}K_{.83})_2B_9O_{15}$, and $(Na_{.80}K_{.20})K_2B_9O_{15}$ were collected in 0.3 mm capillaries on a Stadi P powder diffractometer at room temperature using CuKα$_1$ radiation and a curved PSD detector. The experimental conditions and the crystallographic data are presented in Table 2. The Rietveld refinement was performed using the Rietica program [23]. The atomic positions of $K_3B_9O_{15}$ [18] and the scattering factors for neutral atoms were used as a starting model. The background was modelled using a polynomial approximation with six refined coefficients. The peak profile was described by a pseudo-Voigt function. The positional and thermal displacement parameters were refined for the alkali metal and oxygen atoms. The boron atoms were placed in the centre of the triangles and the tetrahedra built up from oxygen atoms. According to the diffraction data all of the samples contained up to 5 mol% of impurities: $K_5B_{19}O_{31}$ [24] in the case of the samples enriched in potassium, and β-NaB_3O_5 [15] in the case of the sample with the highest sodium content. The second phase was included in the refinement procedure (Table 2). The final positional and thermal displacement parameters and bond lengths and angles are given as supplementary material. Fig. 1 shows the experimental, calculated, and difference XRD patterns after a final Rietveld refinement circle.

2.3. High-temperature X-ray diffraction

The thermal behaviour of the solid solutions was studied in air by in situ HTXRD. The diffraction data were collected on a DRON-3 diffractometer with the high-temperature KRV-1100 attachment (35 kV, 20 mA; CuKα-radiation, graphite monochromator and scintillation detector) according to the

Table 2
Crystal data for $NaK_2B_9O_{15}$, $Na(Na_{.17}K_{.83})_2B_9O_{15}$, and $(Na_{.80}K_{.20})K_2B_9O_{15}$ compared to $K_3B_9O_{15}$

Formula (from structure refinement)	$Na(Na_{.17}K_{.83})_2B_9O_{15}$	$NaK_2B_9O_{15}$	$(Na_{.80}K_{.20})K_2B_9O_{15}$	$K_3B_9O_{15}$ [18]
Crystal system	Monoclinic	Monoclinic	Monoclinic	Monoclinic
Space group	$P2_1/c$	$P2_1/c$	$P2_1/c$	$P2_1/c$
Z	4	4	4	4
a, Å	9.0559 (1)	9.1158 (1)	9.1534 (1)	9.319 (1)
b, Å	6.6170 (1)	6.6246 (1)	6.6296 (7)	6.648 (1)
c, Å	20.5833 (4)	20.6812 (3)	20.7422 (3)	21.094 (2)
β, °	94.228 (2)	94.080 (1)	94.071 (1)	94.380 (9)
V, Å^3	1230.0 (5)	1245.8 (5)	1255.4 (5)	1303.1 (5)
R_{wP}	0.068	0.059	0.052	
R_p	0.053	0.047	0.041	
R_{exp}	0.026	0.020	0.028	
R_B	0.026	0.026	0.023	0.035 (R_F)
Impurities	2.5 mol% β-NaB_3O_5 + unknown phase (traces)	1.7 mol% $K_5B_{19}O_{31}$ + amorphous phase	3.6 mol% $K_5B_{19}O_{31}$	
N[a] (K1/Na1)	0.82(1)/0.15(1)	1/0	1/0	
N[a] (K2/Na2)	0.82(1)/0.17(1)	1/0	1/0	
N[a] (K3/Na3)	0/1	0.05(1)/0.98(1)	0.20(1)/0.80(1)	
Initial charge composition, mol% $K_3B_9O_{15}$	55	75	80	100

[a]Site occupancy from Rietveld refinement.

procedure described in [25]. The sample was prepared from a suspension of heptane on a Pt plate. The measurements were taken between room temperature and the decomposition temperatures up to 800 °C. Temperature steps varied from 20 to 40 °C in the interval between 20 and 600 °C, where thermal expansion was investigated. Above 600 °C partial melting was observed and the steps were decreased to between 10 and 0 °C (repeated scan). The average heating rate was about 100 °C/h in the range of 20–600 °C and 30–50 °C/h above 600 °C. Unit-cell parameters at different temperatures were refined by the least-squares method. The main coefficients of the thermal expansion tensor including its orientation relative to the crystallographic axes were determined using a linear approximation of temperature dependencies for the unit-cell parameters in the range of 20–600 °C.

3. Results and discussion

3.1. Structural study

3.1.1. Structure geometry

Cation polyhedra: There are nine symmetrically independent boron atoms in the structure (Fig. 2a). B_2, B_4, B_6, B_7, B_8, and B_9 are coordinated each by three oxygen atoms, whereas B_1, B_3, and B_5 are tetrahedrally coordinated (Table 3). We consider the boron atom positions less well-determined than the other atomic positions owing to the difficulties of locating light elements with X-ray powder diffractometry. Therefore, only averaged ⟨B–O⟩ distances are given here (Table 3). The ⟨B–O⟩ values range from 1.32 to 1.40 Å for the triangles and from 1.44 to 1.47 Å for the tetrahedra (averages: 1.36 and 1.46 Å for triangles and tetrahedra, respectively). These values are close to the average B–O bond lengths mentioned in [26] for triangles (1.370 Å) and tetrahedra (1.476 Å). There are three symmetrically non-equivalent sites (R1, R2, and R3) occupied by alkali metal ions (Na, K). The cations are coordinated by six to eight oxygen atoms (Table 3, Fig. 2b). The evaluation of the bond lengths in the alkali metal polyhedra upon Na–K substitution is shown in Fig. 3 in comparison with $K_3B_9O_{15}$ [18].

Borate anion: The crystal structures of $NaK_2B_9O_{15}$ and $(Na,K)_3B_9O_{15}$ solid solutions are isostructural to $K_3B_9O_{15}$ [18]. The BO_3 triangles and the BO_4 tetrahedra are connected by shared corners to form three independent triborate rings, each of them consisting of two BO_3 triangles and a BO_4 tetrahedron (Fig. 2a). The borate polyhedra are linked in such way that all oxygen atoms are common to two polyhedra. According to the Heller [27] nomenclature, which was refined by Penin and coauthors [19], the asymmetric unit containing three independent triborate groups can be written as 9: ∞^3 [$3(3:2\Delta+T)$], where the BO_4 tetrahedron is denoted as T and the BO_3 triangle as Δ. In accordance with an additional description of the connectivity after Hawthorne et al. [26] this borate anion should be represented as 9B:⟨2Δ□⟩–⟨2Δ□⟩–⟨2Δ□⟩, where Δ again stands for a BO_3 triangle and □ for a BO_4 tetrahedron; the ⟨ ⟩ delimiters indicate that borate polyhedra form a ring, and a "-" sign between two rings indicates that they share one polyhedron. The frameworks of the similar nonaborates $SrLiB_9O_{15}$, $BaNaB_9O_{15}$, and $BaLiB_9O_{15}$ are built up from the same triborate groups although the borate anion notation is slightly different. In [28] the isotypical $R3c$ frameworks of $SrLiB_9O_{15}$, $BaNaB_9O_{15}$, and $BaLiB_9O_{15}$ nonaborates contain

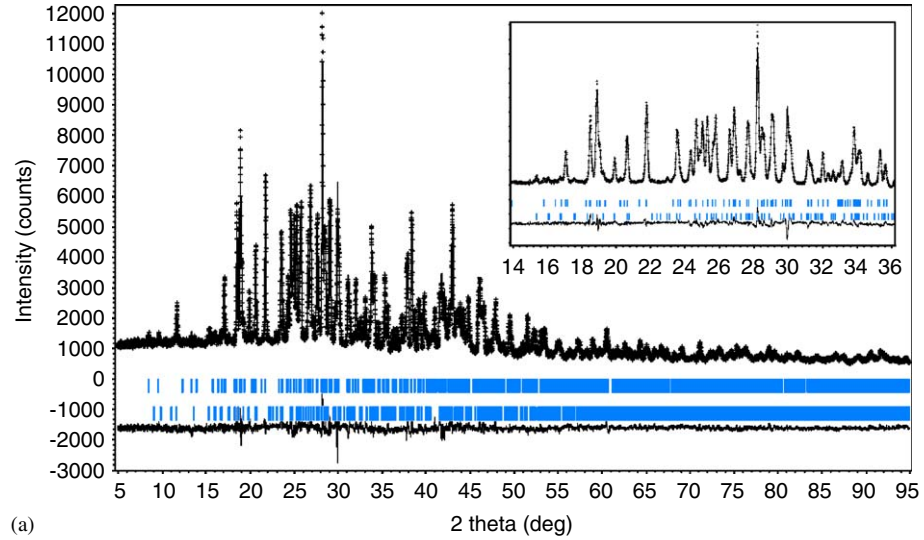

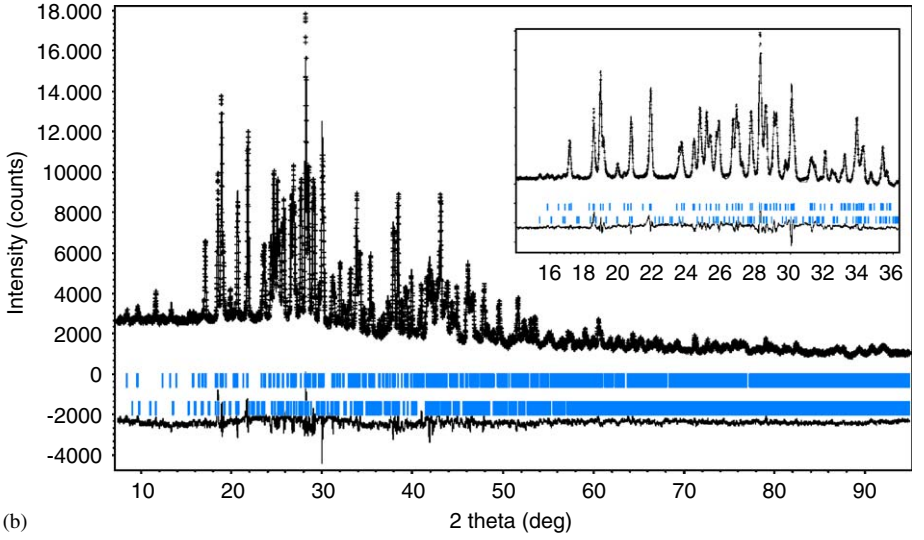

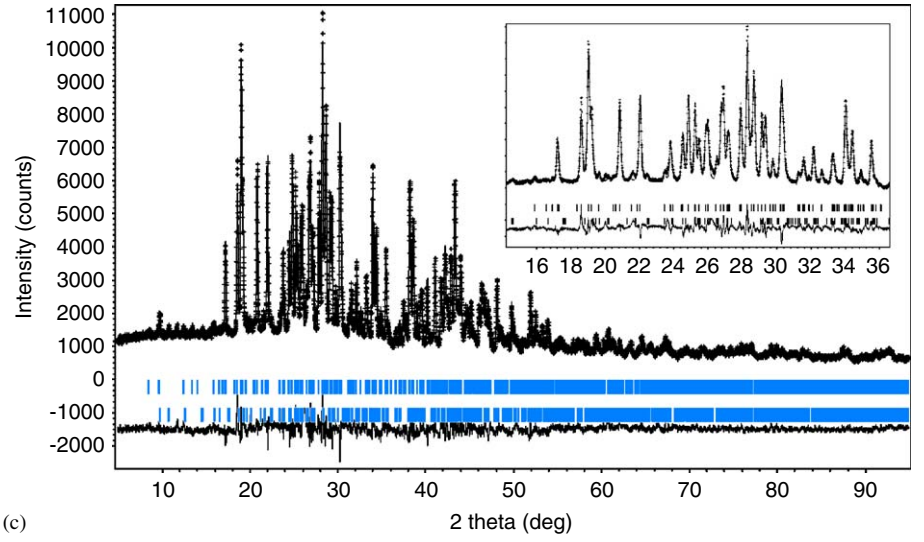

Fig. 1. Rietveld plots for $(Na_{.80}K_{.20})K_2B_9O_{15}$ (a), $NaK_2B_9O_{15}$ (b), and $Na(Na_{.17}K_{.83})_2B_9O_{15}$ (c). +—observed pattern, solid line for simulated pattern, bottom line for difference.

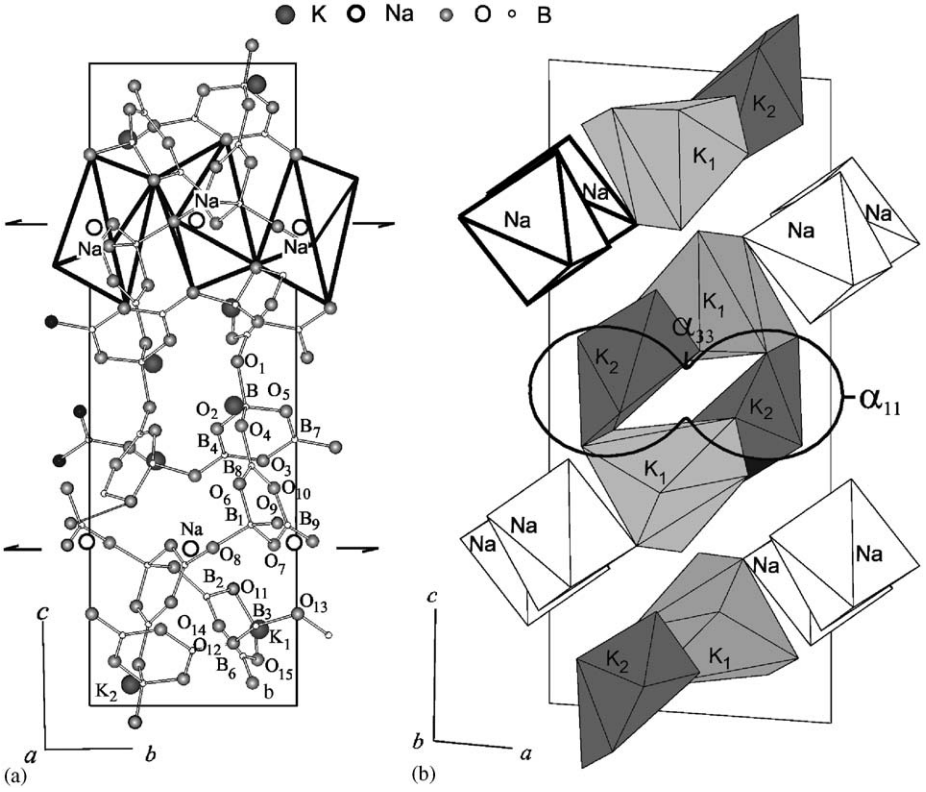

Fig. 2. Crystal structure of $NaK_2B_9O_{15}$. (a) The borate anion and flexible chains from NaO_6 octahedra along *b*; (b) layers built by K(1) and K(2) polyhedra and Na-octahedra chains, and pole figure of the thermal expansion coefficients for $NaK_2B_9O_{15}$.

three independent boron atoms forming one independent triborate ring. According to [19] the notation of borate anion should be written as 9: ∞^3 3[(3 : 2Δ + *T*)]. In [29] the structure of $BaLiB_9O_{15}$ was determined in higher *R*-3*c* symmetry with two independent boron atoms: 9: ∞^3 3[2(1.5 : Δ + 0.5*T*)].

Structure description: The triborate rings are connected by common oxygen atoms and form infinite chains along the 2_1 screw axes. The distance between the nearest alkali metal atoms on R3 varies from 3.53 to 3.57 Å depending on the Na/K ratio in the structure (Table 3). The $R3O_6$ octahedra (NaO_6 in $NaK_2B_9O_{15}$ in Fig. 2a and b) are linked by corners to form flexible chains along the *b* direction. The R1 and R2 cation polyhedra are connected by common oxygen edges into fourfold rings (Fig. 2b). The R1–R2 distances in the ring are 3.53–3.57 and 4.45–4.48 Å. The fourfold rings and octahedral chains are linked by corners to build the layers as shown in Fig. 2b.

3.1.2. *Na/K order–disorder distribution*

Taking into account that in the $K_3B_9O_{15}$ structure [18] there are three structurally independent sites for alkali metal cations (R1, R2, R3), we examined the distribution of Na and K atoms over these sites in the $(Na_{1-x}K_x)_3B_9O_{15}$ nonaborates. We checked two structural possibilities: statistical vs. ordered distribution of K and Na. In both cases the occupancies were refined, whereas the thermal displacement parameters for the cations were constrained to one value. When the refinement of the occupation factors remained stable, the thermal displacement parameters were unconstrained and refined in a separate cycle. Only for the ordered distribution the refinement remained stable and led to reasonable values for the thermal motion of the cations. The Na–K arrangement can be described as follows: if the Na content is less than 1/3, the Na atoms occupy the smallest R3 site only (Table 2) and we have a $(Na,K)K_2B_9O_{15}$ solid solution. For $NaK_2B_9O_{15}$ we observe an ordered Na–K distribution: the R1 and R2 sites are fully occupied by K atoms, and R3 by Na atoms. When increasing the sodium content, we observed Na atoms occupying R1 and R2 sites in a statistically disordered fashion. Among the $Na(Na,K)_2B_9O_{15}$ solutions, $Na_{1.36}K_{1.64}B_9O_{15}$ is the "end member" of the series. In its structure, the R1 and R2 sites are occupied mostly by K atoms, the sodium content at these sites is not above 17%.

If we analyse the size of the cationic polyhedra after substitution of a bigger K atom (crystal radius *R* for coordination numbers 6–8 is 1.52–1.65 Å [30]) with Na ($R = 1.16$ Å for coordination number 6 [30]), significant changes are observed for the smallest R3 site (Table 3, Fig. 3). As K atoms are replaced by Na atoms the mean ⟨(Na,K)–O⟩ bond length decreases from 2.815 Å for the KO_7 polyhedron in $K_3B_9O_{15}$ to 2.490 Å for the NaO_6 polyhedron in $Na(K_{0.17}Na_{0.83})B_9O_{15}$. The coordination number of the alkali metal ion decreases from seven to six. It is known that the ideal coordination number of Na is

Table 3
Selected bond lengths (Å) and angles (deg.) in $NaK_2B_9O_{15}$, $Na(Na_{.17}K_{.83})_2B_9O_{15}$, and $(Na_{.80}K_{.20})K_2B_9O_{15}$ compared with $K_3B_9O_{15}$ [18]

Bond	$Na(Na_{.17}K_{.83})_2B_9O_{15}$	$NaK_2B_9O_{15}$	$(Na_{.80}K_{.20})K_2B_9O_{15}$	$K_3B_9O_{15}$
Individual and mean K,Na–O distances				
R1–O(1)	2.709 (5)	2.761 (5)	2.771 (4)	2.735 (3)
O(2)	2.833 (3)	2.830 (2)	2.757 (2)	2.746 (3)
O(10)	2.915 (4)	2.966 (4)	2.908 (3)	2.909 (3)
O(12)	2.825 (4)	2.866 (3)	2.821 (3)	2.937 (3)
O(8)	3.132 (4)	3.099 (4)	3.078 (3)	2.966 (3)
O(4)	3.003 (4)	2.996 (3)	3.015 (3)	2.992 (3)
O(7)	2.816 (5)	2.850 (4)	2.904 (3)	3.033 (3)
O(14)	3.010 (4)	3.002 (3)	3.042 (3)	3.082 (3)
$\langle R1–O\rangle_8$	2.905	2.921	2.912	2.925
R2–O(6)	2.787 (5)	2.827 (5)	2.820 (4)	2.791 (3)
O(15)	2.852 (3)	2.896 (3)	2.888 (3)	2.854 (3)
O(4)	2.865 (5)	2.918 (4)	2.919 (3)	2.860 (3)
O(12)	2.810 (5)	2.893 (4)	2.897 (4)	2.869 (3)
O(5)	2.908 (3)	2.849 (3)	2.864 (2)	2.903 (3)
O(2)	2.932 (3)	2.946 (3)	2.901 (2)	2.934 (3)
O(1)	2.933 (4)	2.916 (3)	2.903 (3)	2.976 (3)
$\langle R2–O\rangle_7$	2.869	2.892	2.885	2.884
R3–O(11)	2.394 (2)	2.376 (2)	2.375 (2)	2.618 (3)
O(8)	2.338 (3)	2.363 (3)	2.325 (2)	2.619 (3)
O(11)′	2.449 (2)	2.458 (2)	2.504 (2)	2.633 (3)
O(13)	2.415 (5)	2.456 (4)	2.492 (3)	2.807 (3)
O(9)	2.682 (4)	2.731 (3)	2.791 (3)	2.835 (3)
O(3)	2.629 (4)	2.774 (4)	2.818 (3)	2.915 (3)
$\langle R3–O\rangle_6$	2.485	2.526	2.551	2.738
R3–R3′	3.542	3.530	3.547	3.571
R1–R2	4.480	4.452	4.474	4.478
R1–R2′	3.700	3.704	3.705	3.740
R3–O(11)–R3′	94.0	93.8	93.32	85.7
Mean B–O distances in tetrahedra				
$\langle B(1)–O\rangle$	1.469	1.456	1.450	1.472
$\langle B(3)–O\rangle$	1.457	1.460	1.456	1.471
$\langle B(5)–O\rangle$	1.436	1.450	1.458	1.473
$\langle B–O\rangle_4$			1.455	
Individual B–O distances for BO_4			1.403(2)–1.516(2)	
Mean B-O distances in triangles				
$\langle B(2)–O\rangle$	1.379	1.398	1.379	1.371
$\langle B(4)–O\rangle$	1.322	1.328	1.370	1.369
$\langle B(6)–O\rangle$	1.345	1.322	1.349	1.368
$\langle B(7)–O\rangle$	1.379	1.349	1.352	1.370
$\langle B(8)–O\rangle$	1.368	1.353	1.362	1.369
$\langle B(9)–O\rangle$	1.324	1.339	1.367	1.369
$\langle B–O\rangle_3$			1.355	
Individual B–O distances for BO_3			1.249(2)–1.419(1)	

6.4, whereas that of K is 7.9 [31]. The mean bond lengths in the R1 and R2 polyhedra are far less sensitive to the Na–K substitution. This is clearly caused by the character of the K–Na distribution over the different sites. By further increasing the Na content, the R1 and R2 polyhedra decrease. It should be noted that we observe a slight decrease in R3 polyhedra even when their occupation does not change any more. This fact is in accordance with the rule of structural diversity proposed in [32].

Analysing the change of the unit-cell parameters after Na–K substitution (Fig. 4) it was observed that the *b* parameter does not change significantly, whereas the $\langle$(Na,K)–O$\rangle$ distances increase sharply for the R3-polyhedra (Table 3, Fig. 3). This can be explained by decreasing R3–O(11)–R3′ angles between the $R3O_6$ octahedra in flexible chains (Table 3, Fig. 2, NaO_6).

3.2. High-temperature X-ray diffraction studies

3.2.1. Thermal expansion of the (Na,K)-nonaborates

The coefficients of thermal expansion for $K_3B_9O_{15}$, $NaK_2B_9O_{15}$, and $Na(Na_{.17}K_{.83})_2B_9O_{15}$ are given in

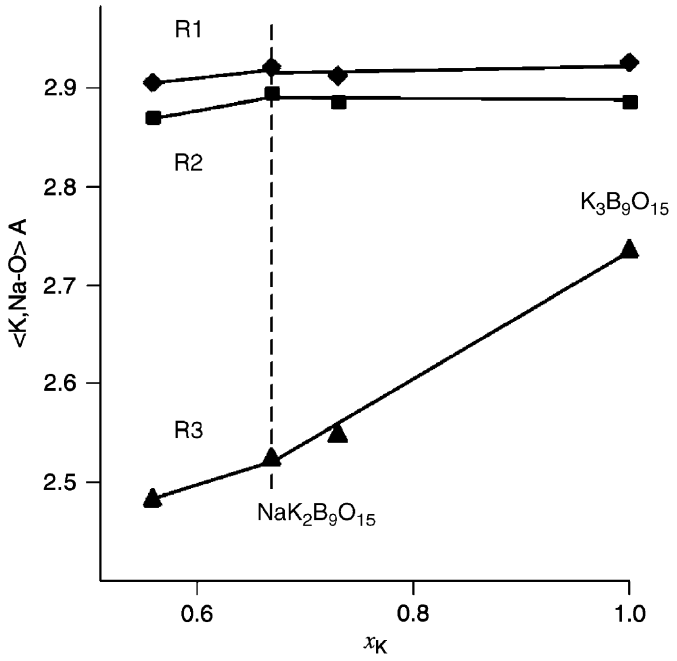

Fig. 3. The average ⟨K,Na–O⟩ distances in R1, R2, and R3 polyhedra as a function of chemical composition. E.s.d. for the cell parameters is comparable with the size of the data points.

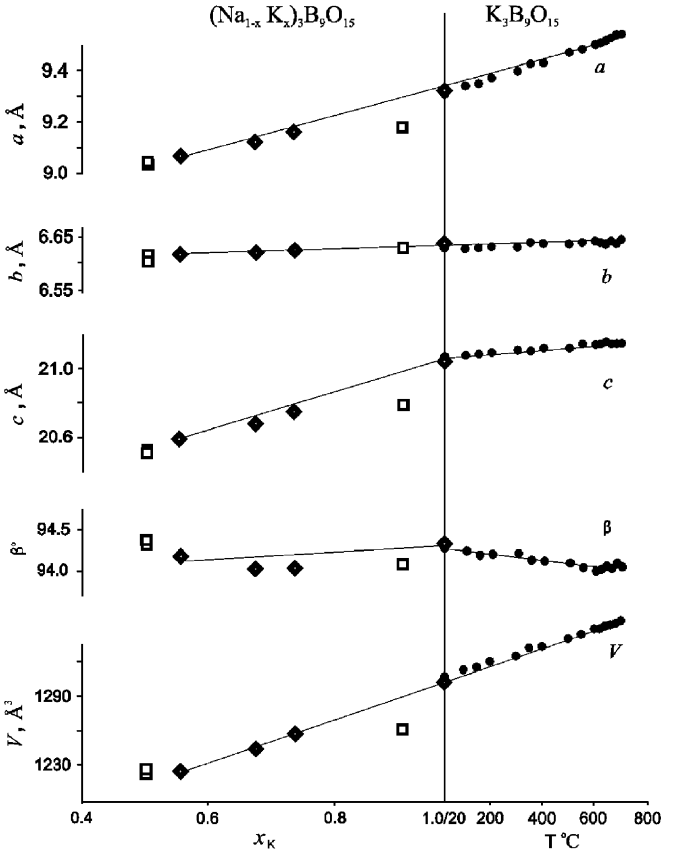

Fig. 4. Similarity of $K_3B_9O_{15}$ structure deformation under K–Na substitution (left) and under heating (right). E.s.d. for the cell parameters is comparable with the size of the data points. □—cell parameters at room temperature; chemical composition is given in accordance to synthesis, ◇—the same; chemical composition is given in accordance to Rietveld refinement, ●—cell parameters at high temperatures by HTXRD.

Table 4. α_{11}, α_{22}, α_{33} are the main coefficients of the tensor, μ ($c\hat{}\alpha_{33}$)° is the angle between the c-axis and the α_{33} tensor axis (anti-clockwise), and the average and volume coefficients are defined as $\alpha_{average} = (\alpha_{11} + \alpha_{22} + \alpha_{33})/3$ and $\alpha_V = \alpha_{11} + \alpha_{22} + \alpha_{33}$. In the monoclinic system one of the main axes of the thermal expansion tensor, α_{22}, is equal to α_b. Two other main directions, α_{11} and α_{33}, are located in the ac monoclinic plane. In the case of the title compounds the monoclinic angle is close to 90° ($\beta \approx 94°$) and μ is close to 0° (Table 4) and owing to this, α_{11} and α_{33} are close to α_a, and α_c, respectively.

Thermal dependencies of the unit-cell parameters for $K_3B_9O_{15}$ are shown as an example in Fig. 4 (right side); the pole figure of the thermal expansion coefficients for $NaK_2B_9O_{15}$ is shown in Fig. 2b. The thermal expansion is similar in all samples studied. It is highly anisotropic (Table 4): the expansion along α_{22}, α_{33}, (along b and approx. c) is low ($\alpha_{min} = 1–5 \times 10^{-6}/°C$), whereas the maximum α_{11} expansion ($37–50 \times 10^{-6}/°C$) nearly coincides with the a-axis.

3.2.2. Compositional vs. thermal deformation in nonaborates

It is well-known [32–35] that in compounds with mainly ionic character the replacement of a smaller cation by a bigger one changes the crystal structure in a similar way to heating. The coefficient of the thermal expansion $\alpha_a = (1/a)(da/dT)$ is analogous to the coefficient of the compositional deformation $\gamma_a = (1/a)(da/dx)$, where x is a characteristic of the chemical composition [34].

In Fig. 4 the compositional deformations of the nonaborates are compared with the thermal expansion using the procedure developed by Filatov [34]. Compositional dependencies of the cell parameters for $(Na_{1-x}K_x)_3B_9O_{15}$ ($x = 0.4–1.0$) were approximated linearly: $a = 8.711(9) + 0.61x$, $b = 6.578(1) + 0.069x$, $c = 19.96(3) + 1.08x$, $\beta = 93.9(3) + 0.4x$, $V = 1134.2(4) + 168(6)x$. The linear equations for temperature dependence of the $K_3B_9O_{15}$ unit-cell parameters were: $a = 9.299(3) + 0.0.00034T$, $b = 6.630(2) + 0.00002T$, $c = 21.073(5) + 0.00012T$, $\beta = 94.29(2) - 0.00035T$, $V = 1295.6(4) + 0.0597(8)T$, $T = 20–700$ (Fig. 4). The compositional and the thermal deformations of $K_3B_9O_{15}$ lead to similar changes in the a and b parameters, the angle β and the volume. Thus, the structure of the $K_3B_9O_{15}$ type undergoes similar distortions upon heating (Fig. 4, right side) and with increasing the K^+ atom content in $(Na_{1-x}K_x)_3B_9O_{15}$ (Fig. 4, left side). γ_{11}, γ_{22}, γ_{33}, $\gamma_{average}$ γ_V are given in Table 4 for the tensor of the compositional deformation. For compositional deformations μ is approximately 0° and $\gamma_{11} \approx \gamma_a$, $\gamma_{33} \approx \gamma_c$, $\gamma_{22} = \gamma_b$ (Table 4).

For quantitative comparison one can use a compositional equivalent of the thermal deformations, α/γ (0.01 at% K/°C) [34]. The average compositional equivalent of the thermal deformations of the $K_3B_9O_{15}$ structure is calculated to be 0.04%/°C (Table 4,

Table 4
Thermal (α) and compositional (γ) deformation coefficients and their equivalents (α/γ) for $K_3B_9O_{15}$ [18], $NaK_2B_9O_{15}$, and $Na(Na_{.17}K_{.83})_2B_9O_{15}$

Compound	Deformation coefficient						Region
	α_{11}	α_{22}	α_{33}	μ°	$\alpha_{average}$	α_V	T (°C)
Main parameters of the thermal expansion tensor (α, 10^{-6}/°C)							
$Na(Na_{.17}K_{.83})_2B_9O_{15}$	49	5	7	−3	20	61	20–600
$NaK_2B_9O_{15}$	50	5	1	0	19	56	20–650
$K_3B_9O_{15}$ [18]	37	3	6	3	15	46	20–660
	Deformation coefficient						Region
	γ_{11}	γ_{22}	γ_{33}	μ°	$\gamma_{average}$	γ_V	x, at% K
Main parameters of the compositional deformations tensor (γ, 10^{-6}/0.01 at% K)							
$K_3B_9O_{15}$	7	1	5	0	4	13	0.4–1.0
	Deformation coefficient						Region
	$(\alpha/\gamma)_{11}$	$(\alpha/\gamma)_{22}$	$(\alpha/\gamma)_{33}$		$(\alpha/\gamma)_{average}$	$(\alpha/\gamma)_V$	0.4–1.0 at% K
Compositional equivalents of the thermal deformations: α/γ (0.01 at% K/°C)							
$K_3B_9O_{15}$	5	3	1		4	4	20–660 °C

$(\alpha/\gamma)_{average} = (\alpha/\gamma)_V$). This means that heating $K_3B_9O_{15}$ by 1 °C leads to the same deformations as increasing the K^+ atom content in the compounds by 0.04 at%. The closeness of $(\alpha/\gamma)_{11}$ and $(\alpha/\gamma)_{22}$ (0.05 and 0.03 at%/°C) to the average value (0.04 at%/°C) indicates a high degree of similarity of the deformations occurring with changes in temperature and chemical composition. $(\alpha/\gamma)_{33}$ is 0.01 at% K/°C and therefore reduces this similarity.

3.2.3. Melting behaviour

In accordance with structural data (Table 2) we observed the existence of the solid solutions of $(Na_{1-x}K_x)K_2B_9O_{15}$ ($0 \leqslant x \leqslant 1$), $Na(Na_{1-x}K_x)_2B_9O_{15}$ ($0.83 \leqslant x \leqslant 1$), and $NaK_2B_9O_{15}$ (sample no. 5 in Fig. 5, 600 °C) in the KB_3O_5-enriched part of the pseudobinary NaB_3O_5–KB_3O_5 section. In the NaB_3O_5-enriched part of the section two phases, β-NaB_3O_5 (sample no. 12 in Fig. 5, 600 °C) and $Na(Na_{.17}K_{.83})_2B_9O_{15}$, co-exist. Lines 1–5 and 5 and 6 divide different biphasic ranges. Left of the lines 1–6 solid solutions and $K_5B_{19}O_{31}$ occur as it is observed in diffraction patterns of the samples with slightly shifted composition from lines 1 to 6 (samples nos. 3, 4 in Table 1, Fig. 5). At the right side there are solid solutions and $K_2B_4O_7$ as it is observed in sample no. 13 (Table 1, Fig. 5). For the last biphasic sample, the formula $(Na_{0.8}K_{0.2})K_2B_9O_{15}$ was determined from unit-cell parameter values.

In Fig. 6 selective diffraction patterns at different temperatures are shown for two samples in comparison with the DSC data. Potassium nonaborate, $K_3B_9O_{15}$, decomposes according to $K_3B_9O_{15} \rightarrow K_5B_{19}O_{31} + K_2B_4O_7$ at 660 °C. This is consistent with the observation that the binary $K_2B_4O_7$–$K_5B_{19}O_{31}$ system has an eutectic point at 740 °C for 27 $K_2O * 73$ B_2O_3 [20]. As is seen from the HTXRD experiment for $K_3B_9O_{15}$ (Fig. 6a), the diffraction patterns do not change up to 640 °C. At 660 °C, diffraction maxima of $K_5B_{19}O_{31}$ and $K_2B_4O_7$ appear. On further

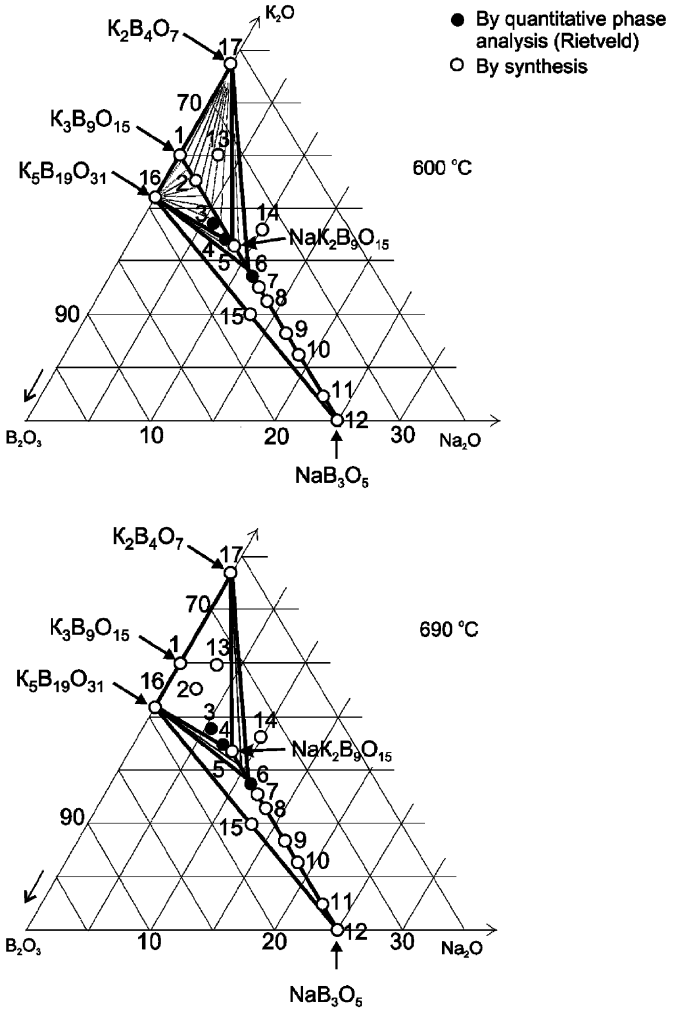

Fig. 5. Subsolidus phase relations in the ternary Na_2O–K_2O–B_2O_3 system at 600 and 690 °C. The figures show the known binary compounds and the ternary compositions investigated by the authors. The numbers refer to the compositions listed in Table 1.

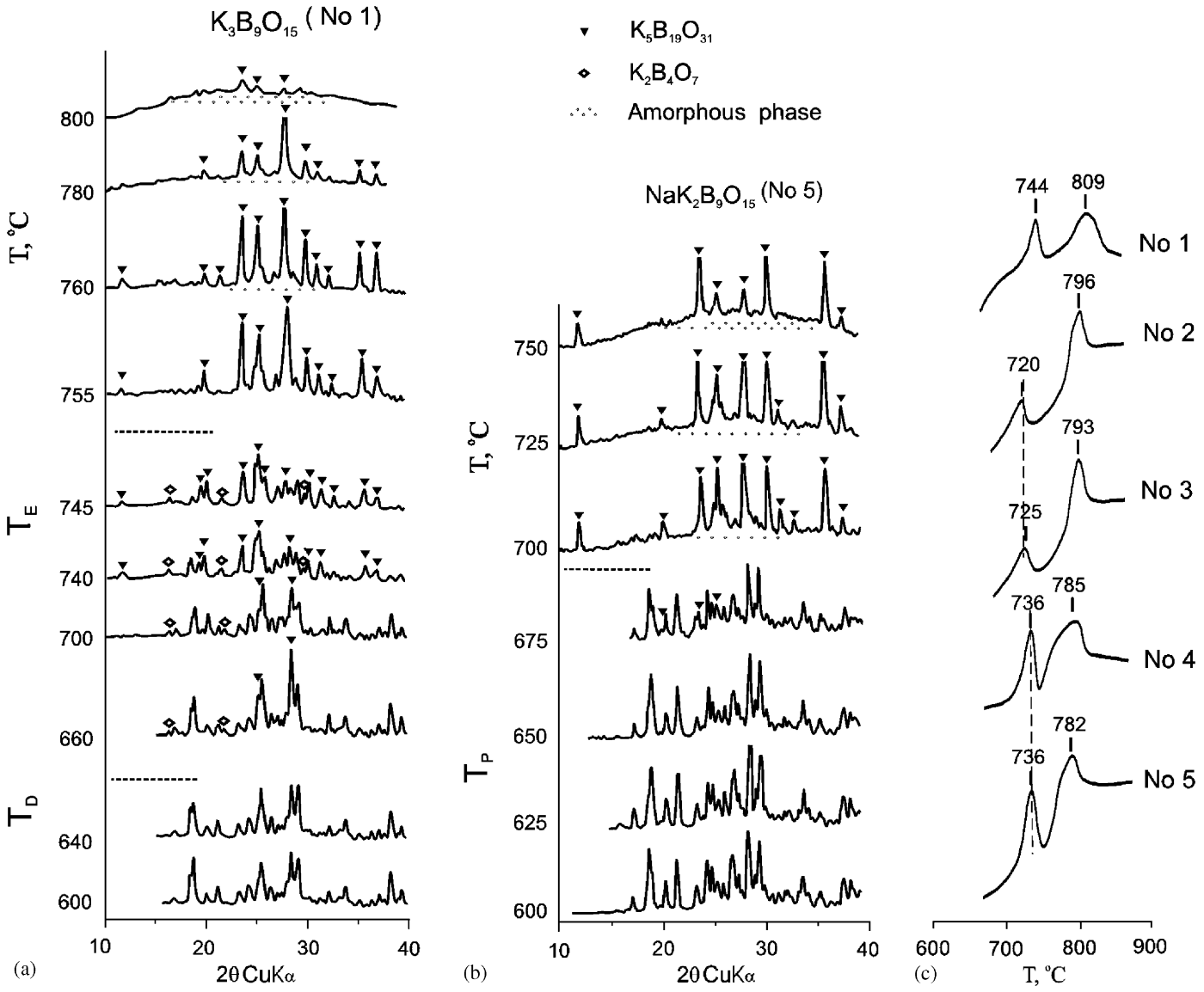

Fig. 6. Selective X-ray diffraction patterns at different temperatures obtained by HTXRD for $K_3B_9O_{15}$ (sample no. 1) (a) and $NaK_2B_9O_{15}$ (sample no. 5) (b) in comparison with the DSC data [21] for samples nos. 1–5 (c).

heating they increase, while reflections of $K_3B_9O_{15}$ decrease sharply and disappear. The decomposition of $K_3B_9O_{15}$ occurs at about (650 ± 10) °C as a result of the solid state reaction mentioned above; the temperature of decomposition T_D is shown by a dashed line in Fig. 6a. At 755 °C, the reflections of $K_2B_4O_7$ disappear and the diffraction pattern of $K_5B_{19}O_{31}$ becomes textured; after further heating the intensity of the reflections decreases and a background which is typical for an amorphous phase (melt) appears. The partial melting point at 750 ± 10 °C is attributed to the melting of a eutectic mixture (Fig. 6a, T_E) in accordance with [25]. Residual $K_5B_{19}O_{31}$ in sample no. 1 is due to its excess in comparison to the stoichiometry of eutectic composition. At 800 °C the peaks of $K_5B_{19}O_{31}$ almost disappear and only an amorphous phase exists (liquidus line). Both temperatures are close to those of endothermic peaks on the DSC curve for $K_3B_9O_{15}$ (Fig. 6c, no. 1).

The solid solutions of $(Na_{1-x}K_x)K_2B_9O_{15}$ $(0 < x \leqslant 1)$ decompose by solid state reaction into three phases at about 650–670 °C $(Na_{1-x}K_x)K_2B_9O_{15} \rightarrow K_5B_{19}O_{31} + NaK_2B_9O_{15} + K_2B_4O_7$ as was shown by annealing in Ref. [21]. The biphasic samples nos. 3 and 13 decompose similarly. $NaK_2B_9O_{15}$ does not decompose, its HTXRD patterns do not change up to the melting temperature (Fig. 6b), the same holds for the biphasic sample no. 4 containing $NaK_2B_9O_{15}$ and traces of $K_5B_{19}O_{31}$. The three-phase ranges containing $K_5B_{19}O_{31}$, $NaK_2B_9O_{15}$, and $K_2B_4O_7$ are limited by $K_5B_{19}O_{31}$–$NaK_2B_9O_{15}$, $NaK_2B_9O_{15}$–$K_2B_4O_7$, and $K_5B_{19}O_{31}$–$K_2B_4O_7$ quasidouble systems (Fig. 5, 690 °C).

In contrast with eutectic melting of $K_3B_9O_{15}$ (Fig. 6a, sample no. 1) mentioned above, $NaK_2B_9O_{15}$ melting is here considered as peritectic on the basis of HTXRD data (Fig. 6b, sample no. 5). HTXRD studies demonstrate that,

at 700 °C, maxima of $NaK_2B_9O_{15}$ decrease drastically and maxima of $K_5B_{19}O_{31}$ appear. After further heating, an elevated background typical of an amorphous liquid phase appears and a texture of $K_5B_{19}O_{31}$ forms. The occurrence of $K_5B_{19}O_{31}$ and the amorphous material can be attributed to the peritectic reaction $NaK_2B_9O_{15} \rightarrow \text{liquid} + K_5B_{19}O_{31}$ (Fig. 6b, T_P). Similar changes of diffraction patterns were observed during melting of the biphasic sample no. 4 with a composition close to $NaK_2B_9O_{15}$. The peritectic temperature is determined in both samples as 700 ± 15 °C. The temperature of the first endothermic peak (736 °C) on the DSC curves for the samples nos. 4 and 5 (Fig. 6c) is attributed to peritectic melting. Although it is higher than the temperature of 700 ± 15 °C determined from HTXRD it is acceptable, taking into account that the heating rate in the DSC-experiment, 10 deg./min., is faster than in the HTXRD (1 deg./min.). For the sample nos. 2 and 3 (Fig. 6c), the temperature of the first endothermic peak (720 and 725 °C) on the DSC curves is attributed to peritectic melting in the ternary Na_2O–K_2O–B_2O_3 system.

4. Conclusions

Structural studies of $(Na,K)_3B_9O_{15}$ solid solutions led to the discovery of the new compound, $NaK_2B_9O_{15}$, in the ternary Na_2O–K_2O–B_2O_3 system. The compound is isostructural to $K_3B_9O_{15}$. It is formed owing to the ordered distribution of Na and K atoms over the three sites in the crystal structure.

There are two examples of solid solutions, $(Na_{1-x}K_x)K_2B_9O_{15}$ ($0 \leqslant x \leqslant 1$) and $Na(Na_{1-x}K_x)_2B_9O_{15}$ ($0.83 \leqslant x \leqslant 1$), and $NaK_2B_9O_{15}$ between them. Upon heating, the $(Na_{1-x},K_x)K_2B_9O_{15}$ solutions ($x = 0$–1.0) exist up to 650–670 °C and decompose into $K_5B_{19}O_{31}$, $K_2B_4O_7$, and $NaK_2B_9O_{15}$. HTXRD studies demonstrate that the $NaK_2B_9O_{15}$ compound melts in accordance with the peritectic reaction $NaK_2B_9O_{15} \leftrightarrow \text{liquid} + K_5B_{19}O_{31}$.

According to the HTXRD results the thermal expansion of $(Na_{1-x},K_x)_3B_9O_{15}$ solutions is sharply anisotropic: the main coefficients are $\alpha_{11} = 37$–50, $\alpha_{22} = 3$–5, $\alpha_{33} = 1-7 \times 10^{-6}\,°C^{-1}$, $\mu = (c \wedge \alpha_{33}) = 3-3°$. The character of the thermal expansion of $(Na_{1-x},K_x)_3B_9O_{15}$ is similar to structure deformations which occur during Na–K substitution.

Acknowledgments

This research was supported for R.B., M.G., M.K. and S.F. by the Russian Foundation for Basic Research (project # 05-03-33246). We are grateful to the Research Training Centre (GRK 611 "Design and Characterization of Functional Materials") of the Deutsche Forschungsgemeinschaft for travel grants for R.B.

Appendix A. Supplementary data

Supplementary data associated with this article can be found in the online version at doi:10.1016/j.jssc.2006.06.020.

References

[1] S. Lin, Z. Sun, B. Wu, C. Chen, J. Appl. Phys. 67 (1990) 634–638.
[2] Y. Wu, T. Sasaki, S. Nakai, A. Yokotani, H. Tang, C. Chen, Appl. Phys. Lett. 62 (1993) 2614–2615.
[3] P. Becker, Adv. Mater. 10 (1998) 979–992.
[4] H. Hellwig, J. Liebertz, L. Bohaty, J. Appl. Phys. 88 (2000) 240–244.
[5] I. Martynyuk-Lototska, O. Mys, O. Krupych, V. Adamiv, Y. Burak, R. Vlokh, W. Schranz, Integrated Ferroelectics 63 (2004) 99–103.
[6] M. Ihara, M. Yuge, J. Krogh-Moe, Ceram. Soc. Jpn. 88 (1980) 179–184.
[7] J. Krogh-Moe, Acta Crystallogr. B 13 (1960) 889–892.
[8] J. Krogh-Moe, Acta Crystallogr. B 30 (1974) 1178–1180.
[9] J. Tu, D. Keszler, Mater. Res. Bull. 30 (1995) 209–215.
[10] M. Touboul, E. Betourne, G. Nowogrocki, J. Solid State Chem. 131 (1997) 370–373.
[11] M. Krzhizhanovskaya, Yu. Kabalov, R. Bubnova, E. Sokolova, S. Filatov, Crystallogr. Reports 45 (2000) 572–577.
[12] M. Krzhizhanovskaya, R. Bubnova, V. Fundamenskii, I. Bannova, I. Polyakova, S. Filatov, Crystallogr. Reports 43 (1998) 21–25.
[13] G.W. Morey, H.E. Mervin, J. Am. Chem. Soc. 58 (1936) 2248–2254.
[14] A. Rollet, C. R. Acad. Sci. 200 (1935) 1763–1765.
[15] J. Krogh-Moe, Acta Crystallogr. B 28 (1972) 1571–1576.
[16] J. Krogh-Moe, Acta Crystallogr. B 30 (1974) 747–752.
[17] J. Krogh-Moe, Acta Crystallogr. B 14 (1961) 68.
[18] R. Bubnova, V. Fundamensky, S. Filatov, I. Polyakova, Doklady Phys. Chem. 398 (2004) 249–253.
[19] M. Touboul, N. Penin, G. Nowogrocki, SSS 5 (2003) 1327–1342.
[20] I. Polyakova, E. Tokareva, Glass Phys. Chem. 23 (1997) 354–367.
[21] R. Bubnova, M. Georgievskaya, S. Filatov, V. Ugolkov, Glass Phys. Chem. 30 (2004) 551–557.
[22] R. Bubnova, B. Albert, M. Georgievskaya, M. Krzhizhanovskaya, K. Hofmann, S. Filatov, Book of Abstracts of ISBB 05 (2005) Hamburg, p. 69.
[23] Rietica program for Windows. Version 1.7.7. (B. A. Hunter, 1997).
[24] J. Krogh-Moe, Acta Crystallogr. B 30 (1974) 1827–1832.
[25] S.K. Filatov, Russian Chem. Rev. 61 (1992) 1085–1090.
[26] F.C. Hawthorne, P.S. Burns, J.D. Grice, Rev. Mineral. 33 (1996) 41–116.
[27] G. Heller, Topics Curr. Chem. 131 (1986) 39–99.
[28] N. Penin, L. Seguin, M. Tauboul, G. Noworgocki, Int. J. Inorg. Mater. 3 (2001) 1015–1023.
[29] D. Yu. Pushcharovsky, E.R. Gobechia, M. Pasero, S. Merlino, O.V. Dimitrova, J. Alloys Compounds 339 (2002) 70–75.
[30] R.D. Shannon, Acta Crystallogr. A 32 (1976) 751–767.
[31] I.D. Brown, The Chemical Bond in Inorganic Chemistry, Oxford University Press, Oxford, 2002.
[32] R. Bubnova, S. Filatov, Proc. Russian Miner. Soc. 112 (1986) 423–428.
[33] R.M. Hazen, L.W. Finger, Comparative Crystal Chemistry, Wiley, New York, 1982.
[34] S.K. Filatov, High-Temperature Crystal Chemistry, Leningrad Nedra, 1990 (in Russian).
[35] R.M. Hazen, R.T. Downs, High-Temperature and High-Pressure Crystal Chemistry, Reviews in Mineralogy and Geochemistry, V. 41, Mineralogical Society of America, Washington, 2000.